ORIGINAL RESEARCH ARTICLE

Effects of Concentration of Adipic Acid on the Electrochemical Migration of Tin for Printed Circuit Board Assembly

Yi Sing Goh[1,2] · A. S. M. A. Haseeb[3] · Wan Jeffrey Basirun[4,5] · Yew Hoong Wong[1,2] · Mohd Faizul Mohd Sabri[1,6] · Boon Yew Low[7]

Abstract
The continuous advancement in innovative electronic applications leads to closer interconnection spacing and higher electric field density, thus increasing the risk of electrochemical migration (ECM)-related failures. The ECM of tin (Sn) attracts great interest due to the wide use of Sn on the surface of the printed circuit board assembly. In this work, we investigated the effects of adipic acid (1 ppm—saturated concentration) on the ECM of Sn using the water drop test (WDT) at 5 V. In situ observation and ex situ characterization of ECM products were carried out using optical and electrochemical techniques. Results show that the ECM failure probability is higher at intermediate adipic acid concentrations (10 ppm, 100 ppm and 1000 ppm). The major ECM reactions include anodic corrosion and the formation of dendrites, precipitates and gas bubbles. ECM failure does not occur at higher adipic acid concentrations (≥ 5000 ppm) although the anodic corrosion becomes more severe. The complexation of Sn with adipic acid to form Sn adipate complex is suggested as the main factor suppressing ECM failure at higher concentrations (≥ 5000 ppm) by retarding ion transport. The electrochemical parameters (E_{corr} and I_{corr}) do not correlate with the ECM failure probability. They affect the anodic dissolution stage, but not the subsequent stages in the ECM mechanism. In this study, the ion transport stage plays a more significant role in determining the ECM failure probability.

Graphical Abstract
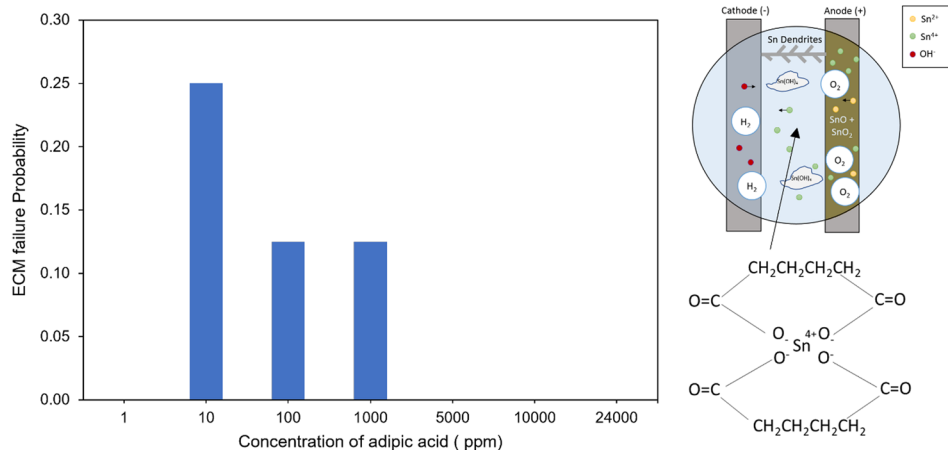
✉ Yi Sing Goh
  yising@um.edu.my

✉ A. S. M. A. Haseeb
  haseeb@nce.buet.ac.bd

Extended author information available on the last page of the article

Introduction

The continuing miniaturization trend, deteriorating service environment and increasing demand for higher performance have elevated the reliability concerns of electronics.[1,2] Higher density in the electronic packages leads to decreased spacing between the conduction terminals and increased electric field intensity. Both conditions give rise to electrochemical migration (ECM)-related failures.[3] ECM is a humidity-induced phenomenon where metal migration occurs in the presence of an electric field and forms conductive dendrites. ECM is highly hazardous to electronics as it can cause short circuits and catastrophic failure of the devices, severely impacting the service life.[4]

Among materials that are susceptible to ECM, tin (Sn) and Sn-based alloys have received extensive interest recently due to their significant role in electronic packaging. For decades, they have been utilized as solder materials, plating for connectors and surface finish on the printed circuit board assembly (PCBA) due to their excellent properties.[5,6] The ECM of Sn can greatly compromise the reliability of electronics, as Sn contributes to a large area of exposed surfaces in the PCBA. The ECM of Sn mainly occurs in four sequential stages: (i) electrolyte formation from moisture content, (ii) anodic dissolution of metallic components to form ions, (iii) ion transport, and (iv) dendrite formation and growth from the reduction of ions.[3,7] As a complex process, ECM can be affected by a combination of factors, including the electric field, spacing between electrodes, temperature, humidity and contaminants.[5,7–11]

The contaminants present in electronics can originate from the manufacturing process, storage and service environment.[12] Their presence could greatly impact the ECM reliability of Sn. For example, some common contaminants like chloride (Cl^-) can accelerate moisture collection and corrosion. It was found that the ECM failure probability of Sn increases with higher Cl^- concentration until a peak value, then decreases due to the formation of excessive precipitates, which hinders ion transport.[13] The ECM failure probability increases again above 0.07 M Cl^- as the precipitates redissolve and form metal ions.[11] A recent study on the bromide ion (Br^-) reported a similar trend, where the anodic dissolution rate increases with Br^- concentration, while ECM failure probability follows a normal distribution first, then increases again above 0.5 M Br^- due to redissolution of the precipitates.[14] Based on these studies, both halides (Cl^- and Br^-) follow a similar ECM mechanism, where at lower concentrations, the anodic dissolution stage is crucial in determining the ECM susceptibility. At higher concentrations, the formation of excessive precipitates in the electrolyte plays a predominant role in the ECM of Sn.

Adipic acid is one of the crucial contaminants found on the surfaces of PCBAs.[15,16] It is utilized as activator in commercial no-clean fluxes to remove metal oxides during the soldering process.[17] Research showed that a large amount (up to 70%) of adipic acid could remain after reflow at 250°C for 45 s (equivalent to maximum reflow temperature and period for lead-free soldering).[18,19] Being hygroscopic in nature, adipic acid can accelerate the electrolyte formation and increase the solution conductivity, hence increasing the risk of corrosion.[17] Existing work related to the ECM of Sn in adipic acid can be grouped into two major types. One type utilized the fluxes containing adipic acid as the activator, while the other focused on the effect of pure adipic acid. The previous ECM work utilizing no-clean fluxes containing adipic acid as the activator showed discrepancies in the explanation of the ECM mechanism. Ambat et al.[15] suggested that ECM of Sn was suppressed due to the passivation effect of adipic acid, resulting in less metal dissolution. Verdingovas et al.[20] showed that the ECM failure probability of Sn decreased above 0.92 g dm^{-3} of the flux residues containing adipic acid as activator. At higher concentrations of flux residue containing adipic acid, more metal ions were formed but were consumed to form the precipitates instead of the dendrites.[20]

Minzari et al.[6] investigated the effects of pure adipic acid on the ECM of Sn at 12 V. ECM failure only occurred at an extremely low concentration (1 ppm) of adipic acid at high bias voltage of 12 V. The authors suggested that at higher concentrations, the adipic acid shifts the bulk pH towards the acidic region and promotes the formation of precipitates.[6] The authors also suggested that higher concentrations of adipic acid suppress the anodic dissolution, thus releasing a smaller amount of metal ions for dendritic growth.[6] The ECM work employing adipic acid as major contaminants has contradictions in explaining the role of adipic acid in the anodic dissolution stage of the ECM mechanism. Ambat et al.[15] and Minzari et al.[6] suggested that higher concentrations of adipic acid suppress anodic dissolution, while Verdingovas et al.[20] explained that more metal ions are formed from anodic dissolution at higher concentrations. Thus, there is a need to clarify the effects of adipic acid on the electrochemical parameters and ECM mechanism. To date, the exact ECM reactions and mechanisms involving adipic acid are still unknown.

A recent study of other weak organic acids (oxalic acid and glutaric acid) shows that the ECM failure probability decreases at higher concentrations of both acids.[21] Oxalate ions actively participate in the ECM mechanism by forming $[Sn(C_2O_4)]^{2-}$ chelate complex with Sn.[21] The subsequent dissociation of the chelate complex controls kinetic factors including mobility and redox rate of Sn cations, thus limiting the reduction of Sn cations to form and grow dendrites.[21] Likewise, adipic acid has also shown complexing ability

with copper (Cu).[22,23] However, the actual conditions and complexing ability of adipic acid are never correlated with the ECM mechanism of Sn, and thus still need to be elucidated. The participation of adipic acid in the ECM reactions should be investigated in-depth to gain an accurate understanding of the mechanisms involved.

Since the anodic dissolution stage is one of the key stages in the ECM process, many researchers have attempted to correlate the electrochemical parameters obtained from potentiodynamic polarization tests with the ECM susceptibility.[5,24–28] Jung et al.[27] reported that the pitting potential (E_{pitt}) of pure Sn in 0.001% Na_2SO_4 is lower compared to 0.001% NaCl (−53.33 mV vs 174.67 mV), while the ECM lifetime of the former is shorter than the latter (40.0 s vs 67.6 s). It was explained that lower anodic dissolution occurs at higher E_{pitt}, which leads to higher corrosion resistance and longer ECM lifetime of Sn. Liao et al.[26] studied the effect of citrate ions on the ECM of Sn with the presence of Cl⁻ ions in the electrolyte. It was found that the formation of Sn-citrate complex occurs in an electrolyte containing 1 mM of citrate ions, resulting in higher E_{pitt}, lower anodic dissolution and the suppression of ECM. Yoo and Kim[29] showed that the ECM failure probability has a linear relationship with the corrosion potential (E_{corr}) and E_{pitt} in electrolytes containing Cl⁻ or SO_4^{2-}. However, a recent study by Lee et al.[14] reported a contradictory result, where E_{corr} and E_{pitt} of Sn decrease with Br⁻ concentration, while ECM failure probability follows a normal distribution, then increases again.

In this work, we study the effects of adipic acid on the ECM reactions of Sn. Systematic variation of adipic acid concentrations over a wide range (1 ppm – 24,000 ppm) is carried out using the water drop test (WDT) at 5 V. The ECM mechanism of Sn in adipic acid is proposed based on the in situ observations and various characterization methods including scanning electron microscopy (SEM), energy dispersive X-ray spectroscopy (EDX), X-ray photoelectron spectroscopy (XPS) and Fourier transform infrared spectroscopy (FTIR). We also elucidate the correlation of electrochemical parameters and ECM susceptibility of Sn in the presence of adipic acid. We find that the adipic acid can suppress ECM failure of Sn at higher concentrations (≥ 5000 ppm) despite more severe anodic dissolution. The electrochemical parameters found through potentiodynamic polarization tests do not correlate with the ECM failure probability when adipic acid is present.

Experimental

Samples and Electrolyte

The samples were pure Sn (> 99.99 wt%) solder bars embedded in epoxy resin. A pair of identical Sn solder bars (0.4 mm × 10 mm × 15 mm) was degreased using soap water and isopropyl alcohol (IPA). A Cu wire was connected to each solder bar at the side using Sn-Bi solders to enable the electrical connections for the subsequent ECM test. The solder bars were embedded in epoxy resin parallel to each other with a gap size of approximately 0.5 mm using a chemically inert polytetrafluoroethylene (PTFE) sheet. Figure 1 shows a schematic diagram of the embedded solder bars. After curing, the sample surface was ground to 3000 grit using silicon carbide (SiC) sandpapers and was polished to 1 μm using polishing cloths and diamond suspension. Prior to the ECM test, the samples were cleaned with distilled water and IPA. The adipic acid solutions were used in the subsequent ECM and potentiodynamic polarization tests. The electrolyte was prepared by mixing distilled water and analytical-grade anhydrous salts stirred at 100 revolutions per minute (rpm). Seven concentrations of adipic acid at 1 ppm, 10 ppm, 1000 ppm, 5000 ppm, 10,000 ppm and 24,000 ppm (saturated concentration) were prepared for these tests.

Water Drop Test

The ECM failure probability and time-to-failure (TTF) of each sample were investigated by conducting an accelerated ECM test which is the WDT. The sample was placed on the platform of a semiconductor characterization system (SCS) (Keithley 4200). The Cu wires on the side of the solder bars were connected to the probes of the SCS. A drop of electrolyte (5 μL) was drop-cast onto the exposed surface of both solder bars as shown in Fig. 2. The bright circular rings in Fig. 2 are the reflections of the optical microscope ring light.

WDT was carried out at a constant bias voltage of 5 V with seven concentrations of adipic acid. During the WDT, a direct current (DC) bias voltage was imposed by the SCS and the compliance was set at 0.02 A. The in situ optical observations were conducted using a microscope attached to the SCS. The current against time data were recorded using the Keithley Interactive Test Environment (KITE) software on a computer. The current surge in the WDT occurred when the ECM product (dendrite) propagated and caused a short circuit by connecting the two terminals. The TTF was the first point where this current surge occurred, indicating the occurrence of a short circuit caused by the first dendrite. For each condition,
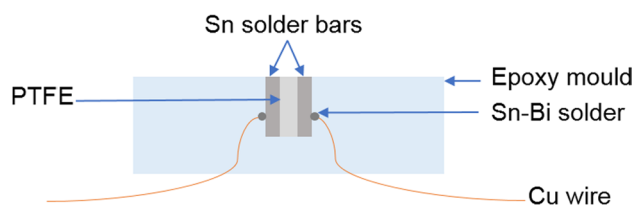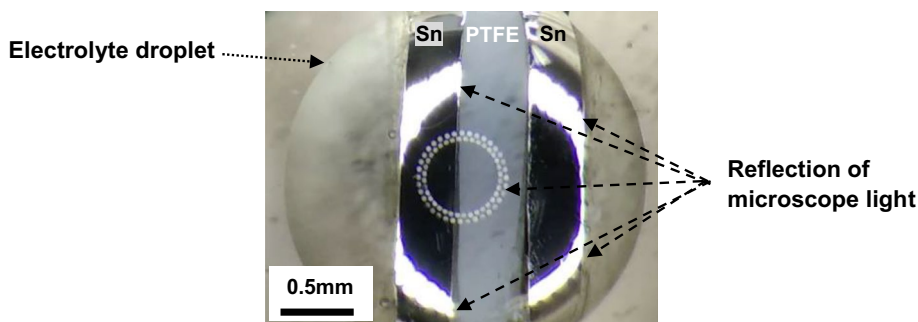

Fig. 1 Schematic diagram of embedded solder bars (side view).

Fig. 2 Optical image of sample surface covered by electrolyte droplet.

eight tests were conducted to calculate the ECM failure probability and the average TTF.

Potentiodynamic Polarization Test

The polarization behaviour of Sn solder bars in different concentrations of adipic acid was investigated using the potentiodynamic polarization test. The potentiodynamic polarization test was conducted using a three-electrode system with a potentiostat (Autolab PGSTAT30, Metrohm Netherlands) connected to a computer. The working, counter and reference electrodes were the Sn solder bar, platinum (Pt) wire and Ag/AgCl electrode in a Luggin capillary, respectively. The linear scan voltammetry was conducted from −1300 mV to +1300 mV at a scan rate of 1 mV s^{-1}.

Characterization of Samples

After the WDT, the morphology of samples such as dendrites and precipitates was investigated using SEM coupled with EDX (Phenom ProX). The microstructural investigation was performed on the SEM micrographs, while EDX was used to identify the elemental composition. XPS of the ECM products formed at the anode was also conducted using the ULVAC-PHI Quantera II. The radiation source was an Al K-alpha monochromatic source (1486.6 eV) with an energy resolution of 1 eV/ step. The XPS was calibrated using the C–C at 284.8 eV as the standard. The elemental curve fitting was performed using MultiPak software (ULVAC-PHI) after the background subtraction. Lastly, FTIR was performed on the ECM products using the PerkinElmer Spectrum 400 to check the adsorption of adipic acid on the sample surface. The FTIR spectra were recorded from 4000 cm^{-1} to 0 cm^{-1} at a resolution of 1 cm^{-1}.

Results

In Situ WDT Results

During the WDT, two types of in situ results are obtained: the current–time plots and the corresponding microscopic observations of the plots. From these results, the ECM failure is confirmed by the occurrence of short-circuiting due to the formation of a dendrite connection between the sample electrodes. Figure 3 shows the typical in situ results obtained from the WDT. The test was performed in 1000 ppm adipic acid at 5 V. The microscopic images at 10 s and 440 s are depicted in Fig. 3a and b to illustrate the changes at different timescales. At 10 s, the polished electrode surfaces remained clean with a few tiny gas bubbles observed on the cathode. At 440 s, numerous small bubbles coalesced to form larger bubbles at the gap between the anode and cathode, while the tiny bubbles were formed and concentrated at the anode. Anodic corrosion was also observed, while the cathodic surface showed the formation of white precipitates, close to the reflection from the optical microscopic light. The formation of thin silvery dendrites connecting the two electrodes was also observed. Figure 3c demonstrates the current–time graph during the WDT of the same sample. The major observation in Fig. 3c was the occurrence of the current surges. The first current surge occurred at around 102.74 s due to the formation of dendrites which connected the gap between the two electrodes and caused the short circuit. The current then dropped significantly, indicating that the dendritic connection had broken. The dendritic connection was either burned off by the high current or destructed by the convective fluid motion.[14,30] At around 196.37 s, another peak representing the second current surge was observed due to the formation of another dendritic connection.

In this work, the concentration of adipic acid is varied from 1 ppm to 24,000 ppm (saturated concentration). The in situ WDT results for 1 ppm, 1000 ppm and 24,000 ppm adipic acid are shown in Fig. 4, as a comparison between the lowest, intermediate and highest concentrations. Figure 4a, b and c illustrate the overlay current–time graphs for 1 ppm, 1000 ppm and 24,000 ppm, respectively. The current–time graphs of the short-circuited samples are excluded from this diagram; otherwise, the sudden current spikes due to short circuits make it difficult to see the trend in the present scale. From these current–time graphs, it is observed that the current passage through the circuit during the WDT increased with higher concentration. The highest concentration of 24,000 ppm showed larger fluctuations compared to the 1 ppm and 1000 ppm graphs. This was due

Fig. 3 In situ results obtained for the sample failed during the WDT carried out in 1000 ppm adipic acid at 5 V. Microscopic observations at (a) 10 s and (b) 440 s and (c) current–time graph. (The bright rings are the reflection from the microscope ring light. − is cathode and + is anode).
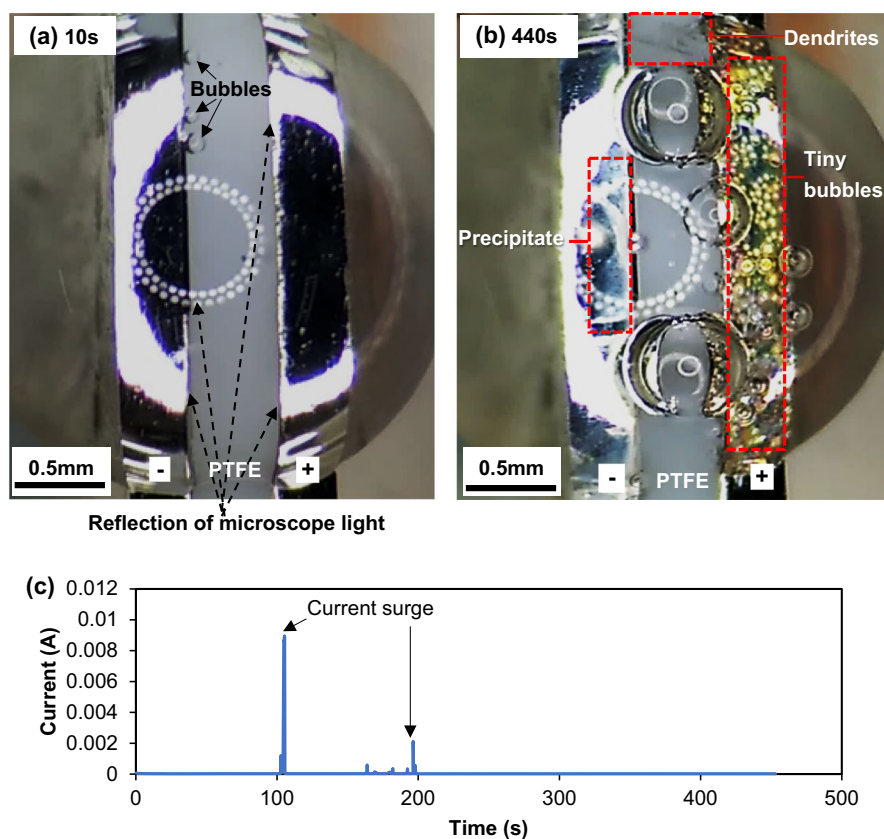
to the continuous cycle of bubble formation, bubble growth and collapse. The microscopic observations at the end of the WDT (440 s) for 1 ppm, 1000 ppm and 24,000 ppm are shown in Fig. 4d, e and f, respectively. The reactions became more vigorous at higher concentrations with increasing bubble formation. Different concentrations of adipic acid also affected the behaviour of the anode. The anode surface remained clean after the WDT at a low concentration of 1 ppm. At 1000 ppm and 24,000 ppm adipic acid, a rainbow-coloured film and a brown film were observed on the anode, respectively. This shows that the anodic corrosion became more severe at 24,000 ppm compared to 1000 ppm, as the rainbow-coloured film at 1000 ppm represented a thinner corrosion product (thin film interference effect). Therefore, the anodic corrosion increased with higher concentrations of adipic acid.

Table I shows a summary of the ECM failure probability and average TTF obtained from the WDT with various concentrations of adipic acid at 5 V. The infinity symbol in the table represents the absence of ECM failure during the entire WDT. The results showed that the ECM mainly occurred at intermediate concentrations (10 ppm, 100 ppm and 1000 ppm). The ECM failure probability was the highest at 10 ppm, followed by 100 ppm and 1000 ppm. The average TTF showed the opposite trend, whereby it decreased from 10 to 1000 ppm. The ECM failure did not occur at a lower concentration (1 ppm) and at higher concentrations (≥ 5000 ppm).

Ex Situ Characterization

After the WDT, the samples were subjected to ex situ characterizations. The samples were left to dry in an ambient atmosphere for two days before the microscopic observations. Figure 5a and b shows the optical micrographs of the completely dried samples after the WDT with 100 ppm and 24,000 ppm adipic acid, respectively. The formation of dendrites and precipitates and the corrosion of the anode were observed for the 100 ppm sample. More severe anodic corrosion was observed for the 24,000 ppm sample. The formation of a white compound was also observed on the sample surface at 24,000 ppm.

The microstructure and composition of the ECM products were investigated using SEM and EDX. Figure 6 shows the SEM images of the WDT test samples at adipic acid concentrations of 1 ppm, 10 ppm, 100 ppm, 1000 ppm, 5000 ppm, 10,000 ppm and 24,000 ppm. The sample surface remained clean with no observable changes at 1 ppm while a light-coloured precipitate was observed at 10 ppm. The formation of precipitates and dendrites was observed at 100 ppm, while the formation of dark phases as the major product was observed from 1000 ppm to 24,000 ppm. The number

Fig. 4 Results obtained for WDT with adipic acid at 5 V. Overlay current–time graphs without short circuit at (a) 1 ppm, (b) 1000 ppm (c) 24,000 ppm. Microscopic images at the end of the WDT for (d) 1 ppm, (e) 1000 ppm, (f) 24,000 ppm. (The bright circular rings are the reflection from the microscope ring light. − is cathode and + is anode).
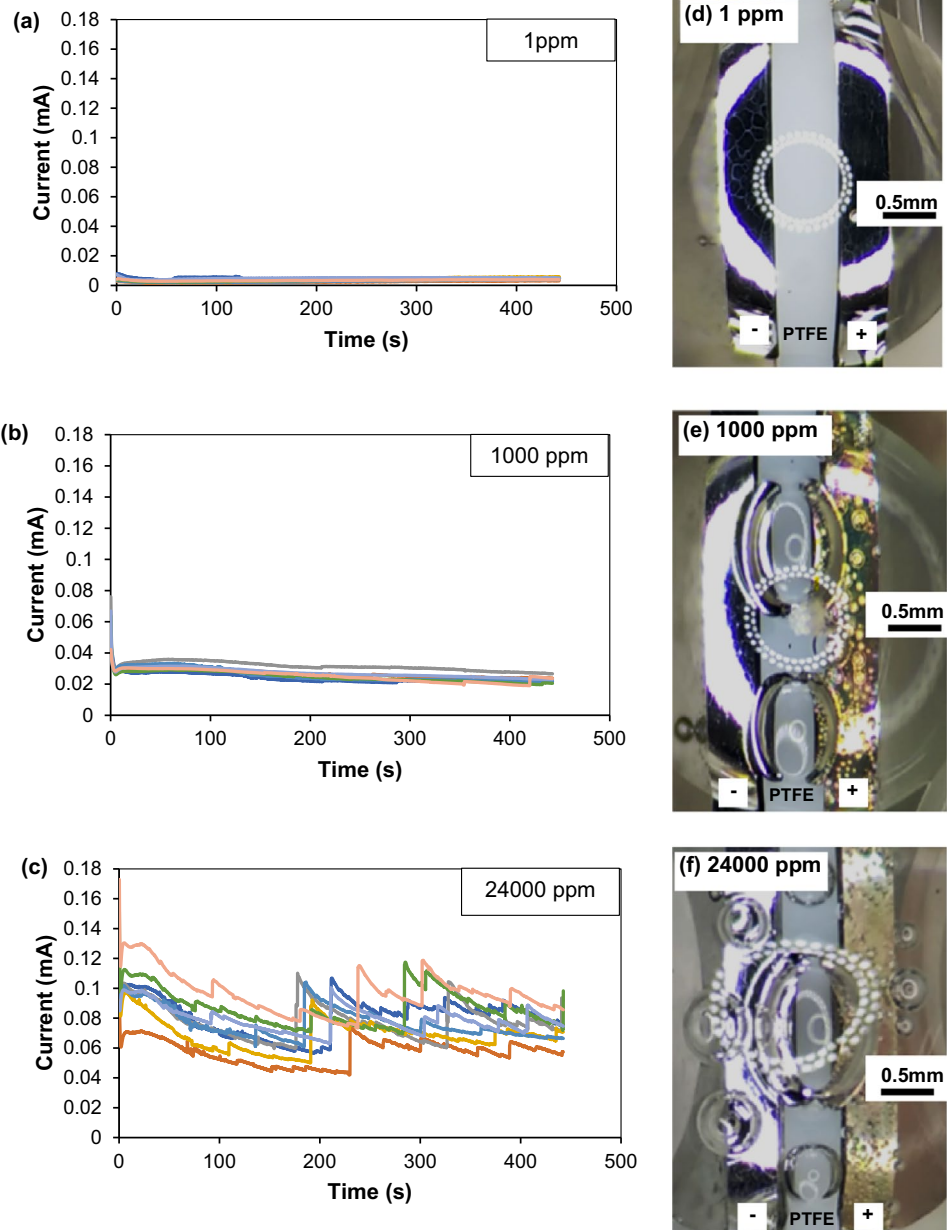

Table I Summary of the ECM failure probability and average TTF obtained from the WDT carried out with various concentrations of adipic acid at 5 V

Concentration (ppm)	ECM failure probability	Average TTF (s)
1	0/8	∞
10	2/8	253.66 ± 110.77
100	1/8	206.62
1000	1/8	102.74
5000	0/8	∞
10,000	0/8	∞
24,000	0/8	∞

of dark phases increased with higher concentration of adipic acid. Numerous dark phases were also observed on the PTFE surface in the space between the two electrodes at 24,000 ppm. The identity of these dark phases was investigated from the comparison between the ex situ microscopic image of 24,000 ppm (Fig. 5b) and the SEM image (Fig. 6g). The white compound in the microscopic images was the only visible product observed in the space between the two electrodes, with a similar shape as the dark phases in the SEM image. Therefore, the white compound in the microscopic image and the dark phases in the SEM image are from the same compound. Further analysis using XPS and FTIR is described in the subsequent section.
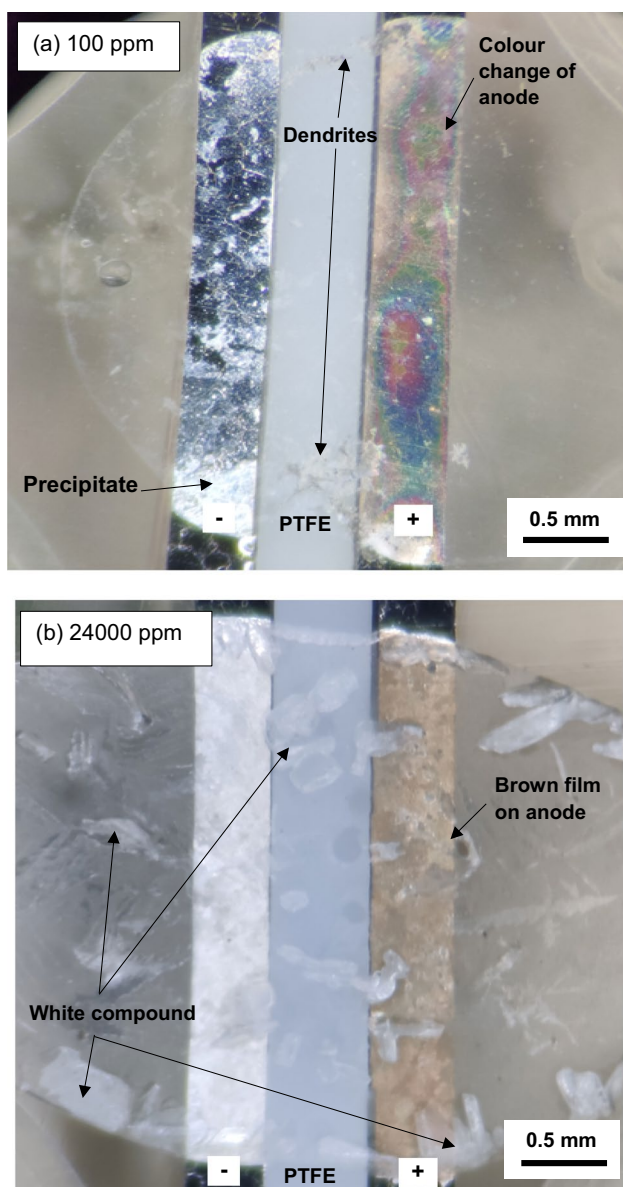
Fig. 5 Microscopic images of the dried samples after the WDT with adipic acid solutions at 5 V (a) 100 ppm and (b) 24,000 ppm (− is cathode and + is anode).

Fig. 6 SEM images of samples that underwent WDT at adipic acid concentrations of (a) 1 ppm, (b) 10 ppm, (c) 100 ppm, (d) 1000 ppm, (e) 5000 ppm, (f) 10,000 ppm and (g) 24,000 ppm (− is cathode and + is anode).

Figure 7a and b demonstrates the SEM images of the dendrites formed at 100 ppm and the dark phase formed at 24,000 ppm, respectively, along with the EDX analysis. The dendrites in Fig. 7a possessed tree-like structures and were surrounded by light-coloured precipitates, while the dark phases in Fig. 7b had a relatively flat surface. The EDX elemental composition analyses of the dendrites, precipitates and dark phases are summarized in Table II. The dendrites consisted mainly of Sn and O, while the light-coloured precipitate consisted of Sn, O and C. The dark phases contained a high amount of C and O. This suggests that the dark phases are likely to be organic compounds, for example,
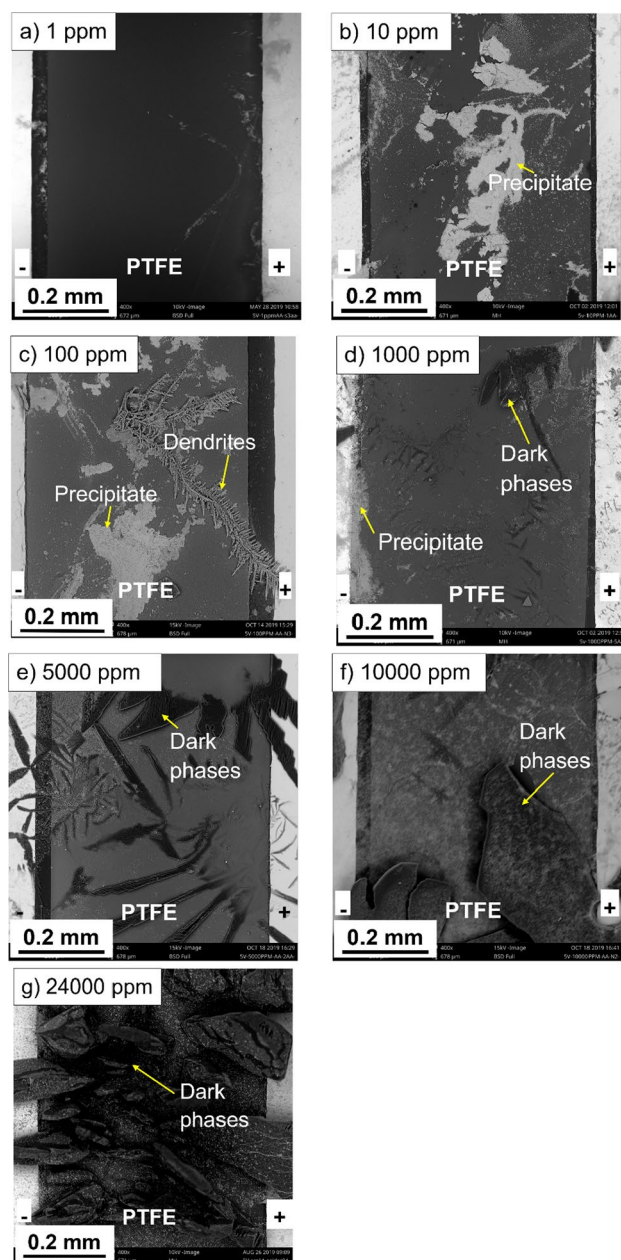
carboxylic acids which contain carboxyl groups (COOH) and their derivatives.

The XPS spectra of the products formed on the anode after the WDT with 24,000 ppm adipic acid (dried, uncleaned) are shown in Fig. 8. From Fig. 8a, the main elements present in the XPS survey spectrum were Sn, O, C and F. The narrow scan was performed to investigate the oxidation states of the Sn, O and C elements. F was excluded from this investigation as it originated from the PTFE
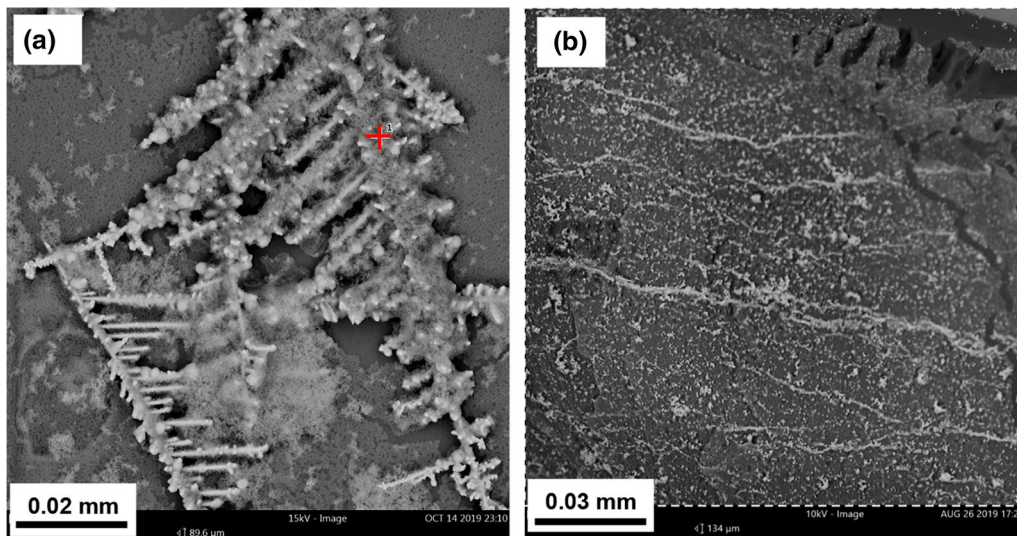
Fig. 7 SEM images at higher magnifications for EDX analysis (a) dendrites formed at 1000 ppm, (b) dark phase formed at 24,000 ppm.

Table II Composition of products based on EDX analysis

Products	Elemental composition (at.%)		
	Sn	O	C
Dendrites	15.57 ± 1.87	84.43 ± 1.87	–
Precipitate	19.63 ± 7.59	69.81 ± 0.82	10.56 ± 7.04
Dark phase	1.85 ± 2.46	27.24 ± 3.18	70.87 ± 4.44

material and not from the reaction products on the anode. Figure 8b shows an asymmetric XPS spectrum of Sn $3d_{5/2}$. This spectrum is composed of two Gaussian functions which are centred at around 486.6 eV and 487.9 eV, representing the Sn^{2+} and Sn^{4+} states, respectively. Figure 8c and d also show an asymmetric pattern of the O 1 s and C 1 s spectra. The spectrum of O 1 s is de-convoluted into three Gaussian functions centred at 530.01 eV, 531.49 eV and 532.73 eV, which represent the O-Sn^{2+}, O-Sn^{4+} and H_2O^+, respectively. The Gaussian functions in the C 1 s spectrum correspond to the -COO-, -C-COO-, -C–C- and -C-H-. Both the Sn and O spectra exhibit higher concentrations of Sn^{4+} compared to Sn^{2+}, suggesting that Sn^{4+} is the major species in the Sn corrosion products. The presence of -COO-, -C-COO- and -C–C- in the narrow scan C spectrum suggests the presence of either carboxylic acid or its derivatives. The carboxylic acid or its derivatives are most probably adipic acid or the derivatives of adipic acid, since the electrolyte was saturated with 24,000 ppm adipic acid. Previous work[31] on anhydrous adipic acid showed a similar narrow scan C spectrum (major peak at 285.0 eV).

To identify the organic compound which appears as a white compound in Fig. 5b and as dark phases in the SEM images, the sample that underwent WDT at 24,000 ppm adipic acid concentration was examined with FTIR. The FTIR spectrum of the products formed after the WDT with 24,000 ppm adipic acid is shown in Fig. 9. The broad peak centred at around 3000 cm^{-1} and a strong sharp peak centred at around 1700 cm^{-1} are attributed to the dimeric H-bond and dimeric C=O stretching, respectively. These are the main characteristics of the FTIR spectrum of a carboxylic acid. The products are suspected to be adipic acid since adipic acid is the only carboxylic acid used in this work. Mouanni et al.[32] reported a similar FTIR spectrum of adipic acid (broad peak at around 3000 cm^{-1} and intense peak at around 1700 cm^{-1}). An additional FTIR analysis was carried out on analytical-grade anhydrous adipic acid and the FTIR spectrum of pure adipic acid obtained in this work is shown in Fig. 9 for comparison. The FTIR spectra of the products and pure adipic acid are almost identical, confirming that the organic compound is adipic acid which crystallizes after the WDT.

Electrochemical Behaviour of Sn in Adipic Acid

Figure 10 shows the polarization curves for Sn in various concentrations of adipic acid. The electrochemical parameters including corrosion potential (E_{corr}) and corrosion current (I_{corr}) were obtained from Fig. 10 and tabulated in Table III. It is obvious that the I_{corr} increases with higher concentrations of adipic acid. The E_{corr} is generally more negative at higher concentrations of adipic acid (from 5000 ppm to 24,000 ppm).
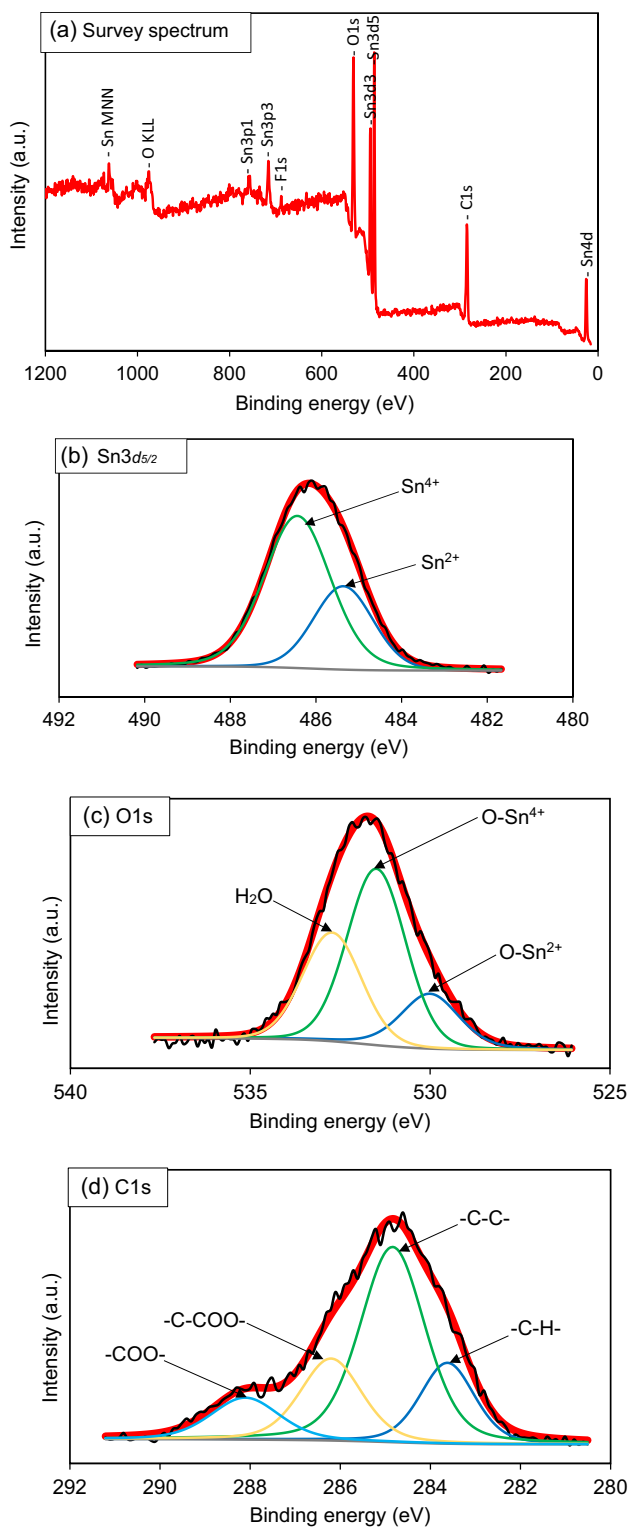
Fig. 8 XPS survey scan of products on the anode after the WDT with 24,000 ppm adipic acid concentration at 5 V (a) Full range XPS survey spectra, (b) Narrow spectrum of $Sn3d_{5/2}$, (c) Narrow spectrum of O1s and (d) Narrow spectrum of C1s.

Discussion

Reactions during ECM

The major reactions described in this work are anodic corrosion and the formation of dendrites, precipitates and gas bubbles. Anodic corrosion is observed in the microscopic images (Figs. 3, 4 and 5), and its severity increases with higher concentration. The XPS spectrum confirms that both Sn^{2+} and Sn^{4+} are present at the anode, with higher concentrations of Sn^{4+}. This suggests that the anodic corrosion of Sn resulted in the formation of SnO_2 and SnO. The presence of SnO_2 is more prominent than SnO, since the former is thermodynamically more stable with a lower standard enthalpy of formation $(\Delta\,°H_f)$ $(-577.63\pm0.20\ kJ\ mol^{-1})$ than the latter $(-280.71\pm0.20\ kJ\ mol^{-1})$.[33] The formation of gas bubbles on the anodic surface during the WDT is attributed to the release of O_2 from the dissociation of water.[34,35] The major reactions at the anode are as follows:

$$Sn \rightarrow Sn^{2+} + 2e^- \tag{1}$$

$$Sn^{2+} \rightarrow Sn^{4+} + 2e^- \tag{2}$$

$$2H_2O \rightarrow 4H^+ + O_2 + 4e^- \tag{3}$$

Gas bubbles are also formed on the cathode surface. This is due to the reduction of H_2O, which releases H_2 and OH^-.[6,26] During the ECM, the electric field causes the negatively charged OH^- ions to migrate to the anode, while the positively charged Sn^{2+} and Sn^{4+} ions are attracted to the cathode. During migration, these ions encounter each other and form precipitates. In this work, the EDX spectrum reveals that the precipitate is mainly SnO_2. The dehydration of $Sn(OH)_4$ releases the SnO_2. This result is in close agreement with previous work which suggested that $Sn(OH)_4$ is the major precipitate formed, owing to the lower solubility product (K_{sp}) of 1.00×10^{-57}.[5,36,37] It is also reported that $Sn(OH)_4$ can be dissociated in acidic medium to form Sn^{4+} due to its amphoteric nature.[5] The dissolution of $Sn(OH)_4$ is expected in this work due to the presence of adipic acid. The water reduction and the formation, dehydration and dissolution of the precipitates are described below:

$$2H_2O + 2e^- \rightarrow H_2 + 2OH^- \tag{4}$$

$$Sn^{4+} + 4OH^- \rightarrow Sn(OH)_4 \tag{5}$$

$$Sn(OH)_4 \rightarrow SnO_2 + 2H_2O \tag{6}$$

Fig. 9 FTIR spectra of the products formed after the WDT with 24,000 ppm adipic acid at 5 V and pure adipic acid.
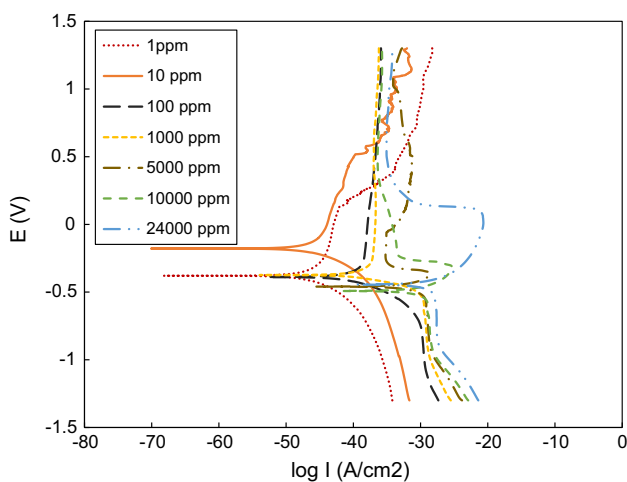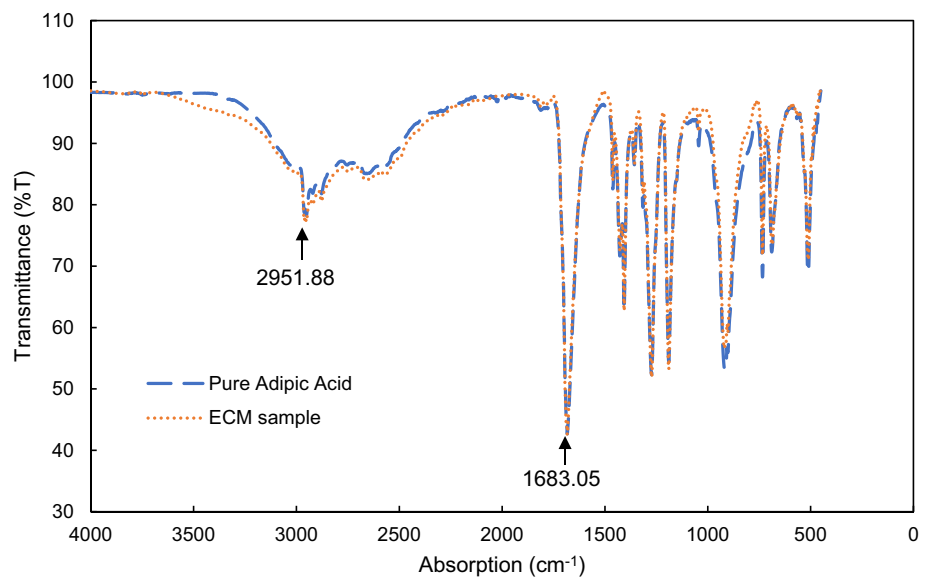

Fig. 10 Polarization curves for Sn at various concentrations of adipic acid (1, 10, 100, 1000, 5000, 10,000 and 24,000 ppm).

Table III Corrosion potential (E_{corr}) and corrosion current (I_{corr}) from different concentrations of adipic acid

Concentration (ppm)	I_{corr} (A/cm^2)	E_{corr} (V)
1	7.41×10^{-8}	−0.397
10	1.09×10^{-7}	−0.179
100	9.61×10^{-7}	−0.389
1000	1.29×10^{-6}	−0.374
5000	3.32×10^{-5}	−0.459
10,000	5.43×10^{-5}	−0.492
24,000	6.93×10^{-5}	−0.444

$$Sn(OH)_4 + 4H^+ \rightarrow Sn^{4+} + 4H_2O \tag{7}$$
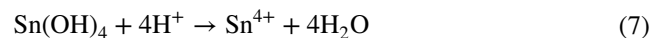
The major reaction at the cathode is the formation of the Sn dendrites. The reduction of Sn^{4+} and Sn^{2+} ions to form Sn dendrites are shown below:

$$Sn^{2+} + 2e^- \rightarrow Sn \tag{8}$$

$$Sn^{4+} + 4e^- \rightarrow Sn \tag{9}$$

The FTIR spectrum confirms that the white organic compound in Fig. 5b and the dark phases in the SEM images is adipic acid because it shows the same FTIR spectrum as pure adipic acid. It should be noted that this compound appeared after the sample was dried at ambient temperature. As the electrolyte was gradually evaporated, the precipitation resulted in the crystallization of the adipic acid.

There are also some possible reactions such as the formation of the Sn complex other than the reactions described above. The complexation of Sn with dicarboxylic acids in flux residues such as oxalic acid was reported by previous work.[21,38] Gouda et al.[38] reported that Sn forms a complex with the oxalate anions in the pH range of 2 to 6 and the complexation controlled the anodic corrosion. Liao et al.[21] investigated the effect of dicarboxylic acids such as oxalic acid and glutaric acid on the ECM of Sn. They found that Sn oxalate complexes were formed from the reaction of $Sn^{2+} + 2C_2O_4^{2-} \rightarrow [Sn(C_2O_4)_2]^{2-}$ with a high chemical equilibrium constant (K) of 8.91×10^{11}, indicating that the process is thermodynamically favourable. These complexes
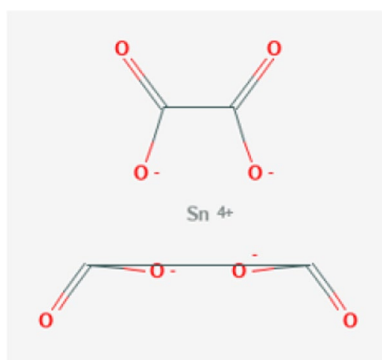
Fig. 11 Chemical structure of dioxalic acid Sn (IV).[39] Reprinted with permission from PubChem.

affect the ECM reaction by suppressing the Sn ion transport and controlling the redox reaction rate.[21] The National Center for Biotechnology Information (NCBI) has included another chemical structure of dioxalic acid Sn (IV) (Fig. 11) in their PubChem database, which is formed from the reaction between Sn and oxalic acid.[39]

At present, there are no detailed investigations on the formation of Sn complexes from the reaction with adipic acid. Important parameters such as K and $\Delta\,^{\circ}H_f$ of the possible Sn adipate complex are still unavailable. However, adipic acid is expected to have a similar tendency as oxalic acid since both are dicarboxylic acids. According to Setifi et al.[22] and Li et al.,[40] adipate is a potential bridging ligand which forms strong surface complexes with metal ions, for example, Cu^{2+} ions and Al^{3+} ions. Singh et al.[41] calculated the stability constants of adipate complexes with various metal ions, such as Zn^{2+}, Ni^{2+} Co^{2+}, Th^{2+} and Cu^{2+}. It is expected that a similar reaction occurs when adipic acid encounters the Sn ions, to form Sn adipate complex. The highly charged Sn^{4+} ions have a tendency to discharge by reacting with the negatively charged $C_6H_8O_4^{2-}$ ions. Thus, it is suggested that the $Sn(C_6H_8O_4)_2$ is formed from the reaction between Sn^{4+} and $C_6H_8O_4^{2-}$.
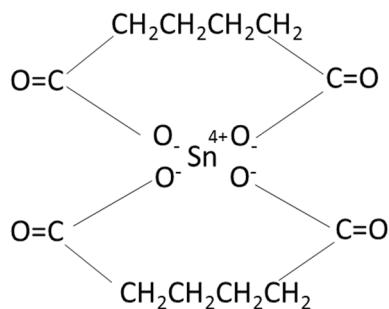

Fig. 12 Proposed chemical structure of the $Sn(C_6H_8O_4)_2$ complex.
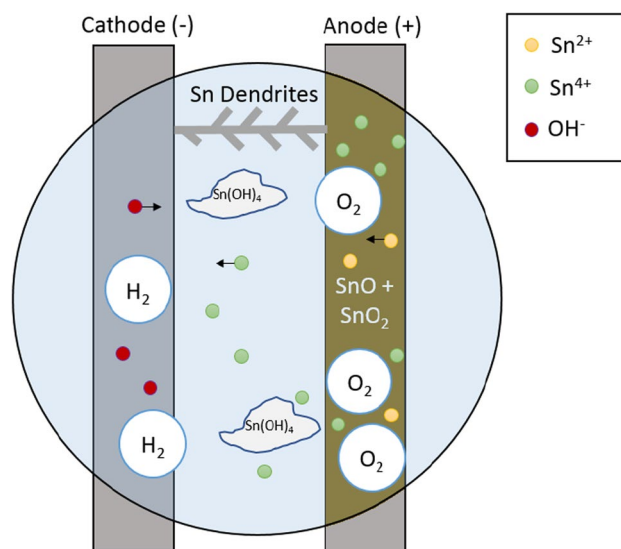
Fig. 13 Schematic diagram of species and compounds formed during the WDT (Top view).

$$Sn^{4+} + 2C_6H_8O_4^{2-} \rightarrow \left[Sn\left(C_6H_8O_4\right)\right]_2 \qquad (10)$$
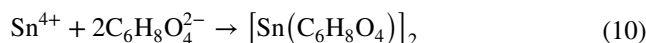
The proposed chemical structure of the $Sn(C_6H_8O_4)_2$ complex is shown in Fig. 12. More in-depth study is required to confirm the formation of this complex. Figure 13 shows a schematic diagram of the species and compounds formed during the WDT with adipic acid.

Effects of Concentration of Adipic Acid

Figure 4a, b and c show that the current passing through the electrolyte increases with higher concentration of adipic acid. At higher concentration, more adipic acid is partially dissociated into the ionic species. Therefore, a higher concentration of adipic acid increases the solution conductivity. Verdingovas et al.[20] also reported that the solution conductivity of the flux residue containing adipic acid increases with higher concentration. From Fig. 4d, e and f, more gas bubbles are observed at higher concentrations of adipic acid. As discussed in Sect. In Situ WDT Results, the anodic corrosion products are thicker at higher concentrations, which suggests that the reaction becomes more vigorous when the concentration of adipic acid increases.

Another notable finding from the SEM images (Fig. 6) is the change in the amount of $Sn(OH)_4$ precipitate with the increase in adipic acid concentration. The amount of $Sn(OH)_4$ precipitate increases from 1 to 100 ppm of adipic acid, then decreases from 1000 ppm to 24,000 ppm of adipic acid. This is due to the pH change of the electrolyte with the increase in adipic acid concentration, as the adipic acid concentration affects solution pH. Adipic acid is a dicarboxylic acid with acidic dissociation constants (K_a) of 4.41 and

5.41.[33] It dissociates in water to form the hydronium (H^+), $C_6H_9O_4^-$ and $C_6H_8O_4^{2-}$ anions. A higher concentration of adipic acid leads to the formation of more H^+ ions, resulting in a lower solution pH. The pH of the adipic acid solution is around 2.7 in the saturated concentration (24,000 ppm) at room temperature.[42] At lower pH, the amphoteric $Sn(OH)_4$ reacts with the acidic medium to form Sn^{4+} ions as shown in reaction (7). This explains the phenomenon where the precipitate becomes less visible above 1000 ppm. Thus, the pH values at 1000 ppm and higher concentrations of adipic acid are in the acidic region.

Table I demonstrates that the ECM failure did not occur at higher concentrations ($\geq$ 5000 ppm) but occurs at intermediate concentrations (10, 100 and 1000 ppm). The average TTF of the failed samples decreases with the increase in adipic acid concentration (10 ppm, 100 ppm and 1000 ppm). This result contradicts the results of Minzari et al.[6] Minzari et al.[6] reported that only 1 ppm adipic acid causes ECM failure with a probability of 2 out of 6, while 10 ppm, 1000 ppm and saturated adipic acid do not show ECM failure. This apparent contradiction could be due to the difference in the applied bias voltage. Minzari et al.[6] conducted the ECM test at 12V while this work used an applied voltage of 5V. The bias voltage accelerates the ECM process by increasing the anodic dissolution and ion migration rates.[8] Since the ECM work of Minzari et al.[6] was conducted at 12V, the reaction rates are expected to be much faster, with ECM failure occurring at a lower concentration of 1 ppm. At high voltage, higher concentrations (10 ppm above) may cause reaction rates that are too high for ECM, leading to high convection or precipitate formation that hinders dendritic growth.[5,35]

Another work by Verdingovas et al.[20] showed a similar trend with this work, where a higher concentration of adipic acid in the flux residues suppresses the ECM failure. Their work using the flux residue mainly containing adipic acid showed that the ECM failure probability was maximum at a peak concentration but decreased beyond the peak concentration. Liao et al.[21] investigated the effect of other weak organic acids (oxalic and glutaric acid) on the ECM of Sn at 3 V. They also observed the same trend, where higher acid concentration suppresses the ECM failure. They suggested that this phenomenon is caused by the formation of Sn complexes from the reaction between the Sn cations and the organic compound anions, which retarded the Sn ion transport. In this work, a similar phenomenon is predicted, where the complexation of Sn with adipic acid occurs in reaction (10) to form the Sn adipate complexes. This phenomenon is suggested to suppress the ECM failure at higher adipic acid concentrations ($\geq$ 5000 ppm) by retarding the ion transport.

The electrochemical parameters of Sn in adipic acid are summarized in Table III. The I_{corr} of the Sn electrode increases with higher concentration of adipic acid. E_{corr} is generally more negative at higher concentrations of adipic acid. This implies that the anodic dissolution of Sn increases with higher concentration of adipic acid. More Sn^{2+} and Sn^{4+} ions are formed from the anodic corrosion at higher concentrations. These ions are the precursors for the subsequent formation of precipitates and dendrites. The ECM failure probability and average TTF are not influenced by the E_{corr}. This contradicts the previous work that presented a direct relationship between E_{corr} and average TTF.[27] The reason for this is that anodic dissolution is only one of the four ECM stages; hence, it is not the sole factor which determines the entire ECM process. Although more metal ions are formed at higher concentrations of adipic acid, some of these ions are consumed in reaction (10) and do not contribute to dendritic formation. In this work, the ion transport stage plays a more significant role than the anodic dissolution stage in determining the ECM failure probability.

Conclusions

In summary, we demonstrate that the ECM of Sn is suppressed at higher adipic acid concentrations ($\geq$ 5000 ppm), despite the more severe anodic corrosion. The ECM failure only occurs at intermediate adipic acid concentrations (10, 100 and 1000 ppm). We show that the major ECM reactions include anodic corrosion and the formation of dendrites, precipitates and gas bubbles. The complexation of Sn with adipic acid to form the Sn adipate complex is suggested as a secondary reaction with Sn^{4+}. This complexation reaction can be the main factor which suppresses ECM failure at higher adipic acid concentrations ($\geq$ 5000 ppm) by retarding the ion transport. Electrochemical parameters (E_{corr} and I_{corr}) do not correlate with the ECM failure probability. They affect the anodic dissolution stage, but not the subsequent stages in the ECM mechanism. In this work, ion transport plays a more significant role in determining the ECM failure probability. The results of our research will be of relevance to future ECM study of other weak organic acids found in modern commercial no-clean fluxes.

References

1. B. Medgyes, A. Gharaibeh, D. Rigler, and G. Harsanyi, On the electrochemical migration mechanism of gold in electronics-less reliable than expected? *Materials* 14, 5237 (2021).

2. K. Dusek, D. Busek, P. Vesely, M. Placek, T. Reichl, J. Sedlacek, and P. Mach, Analysis of a failure in a molded package caused by electrochemical migration. *Eng. Fail. Anal.* 121, 105128 (2021).

3. B. Illes, B. Medgyes, K. Dusek, D. Busek, A. Skwarek, and A. Geczy, Numerical simulation of electrochemical migration of Cu based on the Nernst-Plank equation. *Int. J. Heat Mass Transf.* 184, 122268 (2022).

4. B.K. Liao, Z.Y. Chen, Q.B. Qiu, and X.P. Guo, Inhibitory effect of cetyltrimethylammonium bromide on the electrochemical migration of tin in thin electrolyte layers containing chloride ions. *Corros. Sci.* 118, 190 (2017).

5. X. Zhong, L. Chen, B. Medgyes, Z. Zhang, S. Gao, and L. Jakab, Electrochemical migration of Sn and Sn solder alloys: a review. *RSC Adv.* 7, 28186 (2017).

6. D. Minzari, M.S. Jellesen, P. Møller, and R. Ambat, On the electrochemical migration mechanism of tin in electronics. *Corros. Sci.* 53, 3366 (2011).

7. S. Zhan, M.H. Azarian, and M.G. Pecht, Surface insulation resistance of conformally coated printed circuit boards processed with no-clean flux. *IEEE Trans. Electron. Packag. Manuf.* 29, 217 (2006).

8. S.-B. Lee, M.-S. Jung, H.-Y. Lee, T. Kang, and Y.-C. Joo, Effect of bias voltage on the electrochemical migration behaviors of Sn and Pb. *IEEE Trans. Device Mater. Reliab.* 9, 483 (2009).

9. S. Lee and R.W. Staehle, Adsorption studies of water on copper, nickel, and iron using the quartz-crystal microbalance technique: assessment of BET and FHH models of adsorption. *Mater. Corros.* 48, 86 (1997).

10. R. Hienonen and R. Lahtinen, *Corrosion and Climatic Effects in Electronics* (Finland: VTT Publications, 2007).

11. X.K. Zhong, G.A. Zhang, Y.B. Qiu, Z.Y. Chen, W.X. Zou, and X.P. Guo, In situ study the dependence of electrochemical migration of tin on chloride. *Electrochem. Commun.* 27, 63 (2013).

12. V. Verdingovas, M.S. Jellesen, and R. Ambat, Impact of NaCl contamination and climatic conditions on the reliability of printed circuit board assemblies. *IEEE Trans. Device Mater. Reliab.* 14, 42 (2014).

13. G. Harsanyi, Irregular effect of chloride impurities on migration failure reliability: contradictions or understandable? *Microelectron. Reliab.* 39, 1407 (1999).

14. E.L. Lee, A. Haseeb, W.J. Basirun, Y.H. Wong, M.F.M. Sabri, and B.Y. Low, In situ study of electrochemical migration of tin in the presence of bromide ion. *Sci. Rep.* 11, 1–15 (2021).

15. R. Ambat, M. S. Jellesen, D. Minzari, U. Rathinavelu, M. A. Johnsen, P. Westermann, and P. Møller, in *Proceedings of the Eurocorr* (2009), p. 6

16. K. Piotrowska, M.S. Jellesen, and R. Ambat, Thermal decomposition of solder flux activators under simulated wave soldering conditions. *Solder. Surf. Mount Technol.* 29, 133 (2017).

17. V. Verdingovas, M.S. Jellesen, and R. Ambat, Solder flux residues and humidity-related failures in electronics: relative effects of weak organic acids used in no-clean flux systems. *J. Electron. Mater.* 44, 1116 (2015).

18. H. Conseil, V. Verdingovas, M.S. Jellesen, and R. Ambat, Decomposition of no-clean solder flux systems and their effects on the corrosion reliability of electronics. *J. Mater. Sci. Mater. Electron.* 27, 23 (2016).

19. K. S. Hansen, M. S. Jellesen, P. Moller, P. J. S. Westermann, and R. Ambat, in *2009 Annual Reliability and Maintainability Symposium* (2009), p. 502

20. V. Verdingovas, M.S. Jellesen, and R. Ambat, Influence of sodium chloride and weak organic acids (flux residues) on electrochemical migration of tin on surface mount chip components. *Corros Eng Sci Technol* 48, 426 (2013).

21. B. Liao, C. Hongyu, C. Zhenyu, and G. Xingpeng, Effect of organic acids on the electrochemical migration of tin in thin electrolyte layer. *Innov. Corros. Mater. Sci.* 9, 74 (2019).

22. Z. Setifi, F. Setifi, M. Ghazzali, M. El-Ghozzi, D. Avignant, O. Pérez, and J. Reedijk, Adipate as a tetradentate bridging ligand: synthesis, structure and properties of Cu(II) and Ni(II) compounds with 2,2′-dipyridylamine as a terminal co-ligand. *Polyhedron* 75, 68 (2014).

23. Y.Q. Zheng, D.Y. Cheng, J.L. Lin, Z.F. Li, and X.W. Wang, Adipato-bridged copper(II) complexes. *Eur. J. Inorg. Chem.* 28, 4453 (2008).

24. B.-I. Noh, J.-B. Lee, and S.-B. Jung, Effect of surface finish material on printed circuit board for electrochemical migration. *Microelectron. Reliab.* 48, 652 (2008).

25. L. Hua and H.N. Hou, Electrochemical corrosion and electrochemical migration of 64Sn-35Bi-1Ag solder doping with xGe on printed circuit boards. *Microelectron. Reliab.* 75, 27 (2017).

26. B. Liao, Z. Chen, Y. Qiu, G. Zhang, and X. Guo, Effect of citrate ions on the electrochemical migration of tin in thin electrolyte layer containing chloride ions. *Corros. Sci.* 112, 393 (2016).

27. J.-Y. Jung, S.-B. Lee, Y.-C. Joo, H.-Y. Lee, and Y.-B. Park, Anodic dissolution characteristics and electrochemical migration lifetimes of Sn solder in NaCl and Na_2SO_4 solutions. *Microelectron. Eng.* 85, 1597 (2008).

28. S.-J. Song, S.-R. Choi, and J.-G. Kim, The effect of organic additives for the prevention of copper electrochemical migration. *J. Electroanal. Chem.* 832, 75 (2019).

29. Y. Yoo and Y. Kim, Influence of electrochemical properties on electrochemical migration of SnPb and SnBi solders. *Met. Mater. Int.* 16, 739 (2010).

30. D. Minzari, M.S. Jellesen, P. Moller, P. Wahlberg, and R. Ambat, Electrochemical migration on electronic chip resistors in chloride environments. *IEEE Trans. Device Mater. Reliab.* 9, 392 (2009).

31. J.M. Ferreira, G.F. Trindade, J.F. Watts, and M.A. Baker, Dicarboxylic acids analysed by x-ray photoelectron spectroscopy, Part IV—hexanedioic acid anhydrous. *Surf. Sci. Spectra* 24, 011104 (2017).

32. S. Mouanni, D. Amitouche, T. Mazari, and C. Rabia, Transition metal-substituted Keggin-type polyoxometalates as catalysts for adipic acid production. *Appl. Petrochem. Res.* 9, 67 (2019).

33. D.R. Lide, *CRC Handbook of Chemistry and Physics*, 90th ed., (Boca Raton: Taylor and Francis, 2004), p.791.

34. Y.R. Yoo and Y.S. Kim, Elucidation of the relationship between the electrochemical migration susceptibility of SnPb solders for PCBs and the composition of the resulting dendrites. *Met. Mater. Int.* 16, 613 (2010).

35. X. Zhong, G. Zhang, Y. Qiu, Z. Chen, and X. Guo, Electrochemical migration of tin in thin electrolyte layer containing chloride ions. *Corros. Sci.* 74, 71 (2013).

36. F. Séby, M. Potin-Gautier, E. Giffaut, and O.F.X. Donard, A critical review of thermodynamic data for inorganic tin species. *Geochim. Cosmochim. Acta* 65, 3041 (2001).

37. J.-Y. Jung, S.-B. Lee, H.-Y. Lee, Y.-C. Joo, and Y.-B. Park, Electrochemical migration characteristics of eutectic Sn-Pb solder alloy in NaCl and Na_2SO_4 solutions. *J. Electron. Mater.* 38, 691 (2009).

38. V.K. Gouda, E.N. Rizkalla, S. Abd-El-Wahab, and E.M. Ibrahim, Corrosion behaviour in organic acid solutions—I. Tin electrode. *Corros. Sci.* 21, 1 (1981).

39. National Center for Biotechnology Information, PubChem Compound Summary for CID 9839089, Tin oxalate, (U.S. National Library of Medicine,2020), https://pubchem.ncbi.nlm.nih.gov/compound/Dioxalic-acid-tin_IV_-salt. Accessed 25 July 2021

40. Y.-D. Li, Y. Zhang, S.-M. Li, and P.-Z. Zhao, Influence of adipic acid on anodic film formation and corrosion resistance of 2024

aluminum alloy. *Trans. Nonferrous Met. Soc. China* 26, 492 (2016).

41. R.K.P. Singh, J.K. Sircar, J.R. Yadava, and K.L. Yadava, Stability constants of adipate complexes of copper(II), nickel(II), zinc(II), cobalt(II), uranyl(II) and thorium(IV) determined by electrophoresis. *Electrochim. Acta* 26, 395 (1981).

42. M. Williams and M.J. O'Neil, *The Merck Index: An Encyclopedia of Chemicals, Drugs, and Biologicals* (Cambridge: Royal Society of Chemistry, 2013), p.30.

Authors and Affiliations

Yi Sing Goh[1,2] · **A. S. M. A. Haseeb[3]** · **Wan Jeffrey Basirun[4,5]** · **Yew Hoong Wong[1,2]** · **Mohd Faizul Mohd Sabri[1,6]** · **Boon Yew Low[7]**

1 Department of Mechanical Engineering, Faculty of Engineering, Universiti Malaya, 50603 Kuala Lumpur, Malaysia

2 Centre of Advanced Materials, Faculty of Engineering, Universiti Malaya, 50603 Kuala Lumpur, Malaysia

3 Department of Nanomaterials and Ceramic Engineering, Faculty of Chemical and Materials Engineering, Bangladesh University of Engineering and Technology, 1000 Dhaka, Bangladesh

4 Department of Chemistry, Faculty of Science, Universiti Malaya, 50603 Kuala Lumpur, Malaysia

5 Nanotechnology and Catalysis Research Centre, Institute for Advanced Studies, Universiti Malaya, 50603 Kuala Lumpur, Malaysia

6 Centre for Energy Sciences, Faculty of Engineering, Universiti Malaya, 50603 Kuala Lumpur, Malaysia

7 NXP Malaysia Sdn Bhd, Sungai Way Free Trade Industrial Zone, 47300 Petaling Jaya, Selangor, Malaysia